Lithium Titanate Tailored by Cathodically Induced Graphene for an Ultrafast Lithium Ion Battery

*Yingchang Yang, Binghan Qiao, Xuming Yang, Laibing Fang, Chengchi Pan, Weixin Song, Hongshuai Hou, and Xiaobo Ji**

Nonoxidative cathodically induced graphene (CIG) here incorporates conductive agents for $Li_4Ti_5O_{12}$ (LTO) anode materials. The tailored LTO/CIG composite is fabricated by controlled hydrolysis of tetrabutyl titanate in the presence of nonoxidative defect-free cathodically induced graphene (CIG) and oxalic acid in a mixed solvent of ethanol and water, followed by hydrothermal reaction and a calcination treatment. Due to the introduction of defect-free graphene, the resulting LTO/CIG composite shows an excellent electrical conductivity (1.2×10^{-4} S cm^{-1}) and Li^+ diffusion coefficient (1.61×10^{-12} cm^2 s^{-1}). As a result, the tuned LTO/CIG composite exhibits outstanding electrochemical performance, including excellent cycling stability (the capacity retention ratios after 500 cycles at 0.5 C is 96.2%) and a remarkable rate capability (162 mAh g^{-1} at 10C, 126 mAh g^{-1} at 100 C). A specific energy of 272 Wh kg^{-1} at power of 136 W kg^{-1} is observed when cycling against Li-foil. Even during 36 s of charge/discharge, the specific energy of LTO/CIG composite remains at 166 Wh kg^{-1}.

1. Introduction

Due to growing demand for modern electric vehicles (EVs), stationary off-peak energy storage systems, intensive research efforts have been developed to design better anode materials of lithium ion batteries (LIBs) in need of high energy/power density, superior safety and long cycle life.[1–5] Although graphite anodes, with large cell voltage, have been extensively applied as anodes in current commercial LIBs, their poor rate capability resulted from their low Li^+ diffusion coefficient (ca. 10^{-10}~10^{-11} cm^2 s^{-1}), serious safety issues induced by solid electrolyte interphase (SEI) film and reduced cycle stability caused by volume change (9~13%) during lithiation/delithiation limit their wide applications in the next generation LIBs.[6–8]

Y. C. Yang, X. M. Yang, L. B. Fang, C. C. Pan, W. X. Song, H. S. Hou, Prof. X. B. Ji
Key Laboratory of Resources Chemistry of Nonferrous Metals
Ministry of Education
College of Chemistry and Chemical Engineering
Central South University
Changsha 410083, China
E-mail: xji@csu.edu.cn
B. H. Qiao
School of Foreign Languages
Central South University
Changsha 410083, China

DOI: 10.1002/adfm.201304263

Lithium titanium oxide with the cubic spinel structure, $Li_4Ti_5O_{12}$ (LTO), has been extensively investigated as anode materials for the next-generation lithium ion batteries because of its intrinsic characteristics, such as the stable charge/discharge platform at 1.5 V vs. Li^+/Li, which is just above the formation of SEI. Also note that it has zero strain features during the lithium intercalation/extraction.[9–14] It was not surprising to see that proprietary nanostructured LTO was firstly introduced to replace the traditional graphite materials in EVs and advanced energy storage systems by Altairnano.[15] Nevertheless, the rate performance of pristine LTO is relatively poor due to its moderate Li^+ diffusion coefficient and low electrical conductivity. It should be pointed out that the LTO-based LIBs suffer from severe gassing during charge/discharge cycles, resulting from interfacial reactions between LTO and surrounding alkyl carbonate solvents, which hinders its large-scale applications in LIBs industries.[16–19] To suppress the gassing issues, an effective strategy of constructing a barrier between the LTO and the surrounding electrolyte solution has been designed.[19]

In terms of the improvement of rate capability, many methods including designing of novel micro-nanostructure, doping with foreign atoms and conductive agents incorporating, have been exploited up to now.[10,13,14] Micro-nanostructured LTO materials, with short transportation distance for both Li^+ and electrons, have been extensively developed to increase the rate capability.[20–24] However, the preparation of these structured materials in large scale is costly and quite challenging. The conductivity and rate performance of LTO can also be tuned by doping some foreign atoms.[10,13,14,25,26] Recently, phosphidated-$Li_4Ti_5O_{12}$ was fabricated by Park et al. via the thermal decomposition of trioctylphosphine.[24] This material with enhanced Li^+ conductivity improved the rate performance to a capacity of 100 mAh g^{-1} at a rate of 10C (1C = 175 mA g^{-1}). This enhancement is meaningful but still not good enough for applications in EVs or large-scale energy storage.

Another good choice to enhance the rate performance is conductive agents incorporating. Graphene, a single-atom-thick sheet of honeycomb carbon lattice, was recently chosen as a conductive additive to improve the capabilities of LTO composites due to its superior electrical conductivity (64 mS cm^{-1}), extremely high theoretical surface area (2675 m^2 g^{-1}) and

mechanical robustness.[27,28] A spinel LTO nanoplatelet/reduced graphite oxide nano-hybrid, designed by Kim et al. with a two-step microwave-assisted solvothermal reaction and heat treatment method, could deliver a discharge capacity of 101 mAh g^{-1} at 100 C.[29] Shen et al. reported a LTO/GNS (graphene nanosheet) nanocomposite synthesized via in situ synthesis using graphite oxide as reaction precursor.[30] This composite showed a discharge capacity of about 90 mAh g^{-1} at a high rate of 60 C. Graphene-supported LTO nanosheets was also prepared by Tang et al. with a facile hydrothermal method.[31] This sample possessed good cycle stability and a high specific capacity of 140 mAh g^{-1} at 20 C.

To the best of our knowledge, the graphene used as conductive additive in these LTO composites was mostly prepared by chemical or thermal reduction of graphite oxide (GO) synthesized from natural graphite powder by a modified Hummers method.[32] These reduced graphene oxides (RGO) inevitably suffer from poor electrical conductivity because of the presence of oxygen functional groups, which will decrease the heterogeneous electron transfer and restrict the high rate performance of LTO/graphene composites electrodes.[33–36] According to our previous results,[35,36] the surfactant impurities in RGO, mainly arising from various preparation processes, including metal oxides or surfactant, have a negative impact on the elcetrochemcial properties of graphene-based energy storage/generation devices. In 2011, Loh and co-workers developed an electrochemical expansion of graphite route to get non-oxidative few-layer graphene (FLG) flakes with the high and prolonged power sonication step.[37] Very recently, our group developed an electrochemically cathodic exfoliation method in room temperature ionic liquids N-Butyl, methylpyrrolidinium bis(trifluoromethylsulfonyl)-imide (BMPTF2N) for few-layer graphene sheets, demonstrating low levels of oxygen (2.7 at% of O) with a nearly perfect structure ($I_D/I_G < 0.05$).[38]

Herein, the nonoxidative cathodically induced graphene (CIG) are exploited as incorporating conductive agents for LTO anodes, aiming at improving the cyclic performance and high rate capability performance of LTO/CIG materials. CIG was fabricated by electrochemically cathodic exfoliation of graphite in room temperature ionic liquids. Controlled hydrolysis of tetrabutyl titanate in the presence of CIG and post treatment was used to prepare the tailored LTO/CIG composite. The as-fabricated LTO/CIG composite, benefiting from the introducing of defect-free CIG with high electronic conductivity, shows low polarization of voltage difference and excellent cycling stability (the capacity retention ratios after 500 cycles at 0.5, 10 and 25 °C are 96.2, 90.3 and 74.6%, respectively). In particular, the rate capability of this composite is marvellous (162 mAh g^{-1} at 10 C, 126 mAh g^{-1} at 100 C) in comparison with the LTO materials reported in the literature so far, when used as anode materials for lithium ion batteries.

2. Results and Discussion

2.1. Material Synthesis and Characterization

Figure 1 illustrates the fabrication of LTO/CIG composite and pure LTO. For the synthesis of composite (Figure 1a),

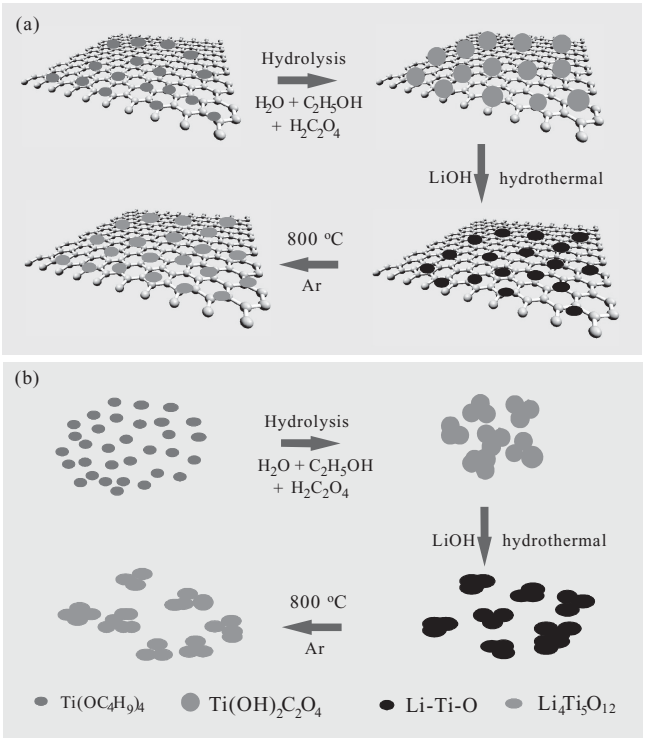

Figure 1. Schematic illustration for the fabrication (a) LTO/CIG composite and (b) pure LTO samples.

ethanol solutions of $Ti(OC_4H_9)_4$ (TBT) was dropwise added into water/ethanol solutions (1:1, in volume) containing OA and CIG, the grey precipitate began to form after 15 min. According the previous work,[39,40] the reaction of Ti^{4+} with oxalic acid would result amorphous hydroxyl tatanium oxalate ($Ti(OH)_2C_2O_4$). Thus, uniform $Ti(OH)_2C_2O_4$/CIG composite was formed during this step. Then, Li-Ti-O/CIG, the precursor of $Li_4Ti_5O_{12}$/CIG composite, was prepared using hydrothermal treatment of the $Ti(OH)_2C_2O_4$/CIG composite. Lastly, the Li-Ti-O/CIG composite was treated at 800 °C for 1 h under Ar atmosphere in order to obtain composite materials composed of uniformly phase-pure and highly crystalline $Li_4Ti_5O_{12}$ and highly conductive CIG. Without the addition of CIG (Figure 1b), the $Li_4Ti_5O_{12}$ particles are easily suffered from agglomeration. This reveals that the graphene can assist the nucleation of $Ti(OH)_2C_2O_4$ when $Ti(OC_4H_9)_4$ is hydrolysed and limit their growth, which is in consistent with the previous reports.[41,42]

The XRD patterns of pure LTO and LTO/CIG composite are shown in **Figure 2**a. As can be seen, the major diffraction peaks for bare LTO at 18.33°, 30.20°, 35.58°, 37.18°, 43.25°, 47.35°, 57.22°, 62.83°, 66.07° and 74.34° can be indexed to (111), (200), (311), (222), (400), (331), (333), (440), (531) and (533) of cubic spinel lithium titanate, $Li_4Ti_5O_{12}$ (JCPDS no. 49-0207).[18,23] For LTO/CIG composite, a small (002) diffraction peak of the disorderedly stacked few-layer graphene sheets appears at 2θ of 26.4°.[37,38] It is observed that the LTO/CIG composite has no other impurities. Also the analysis of thermogravimetric (TG) shows that the graphene content in the LTO/CIG composite is about 3.5 wt.% (Figure 2b).

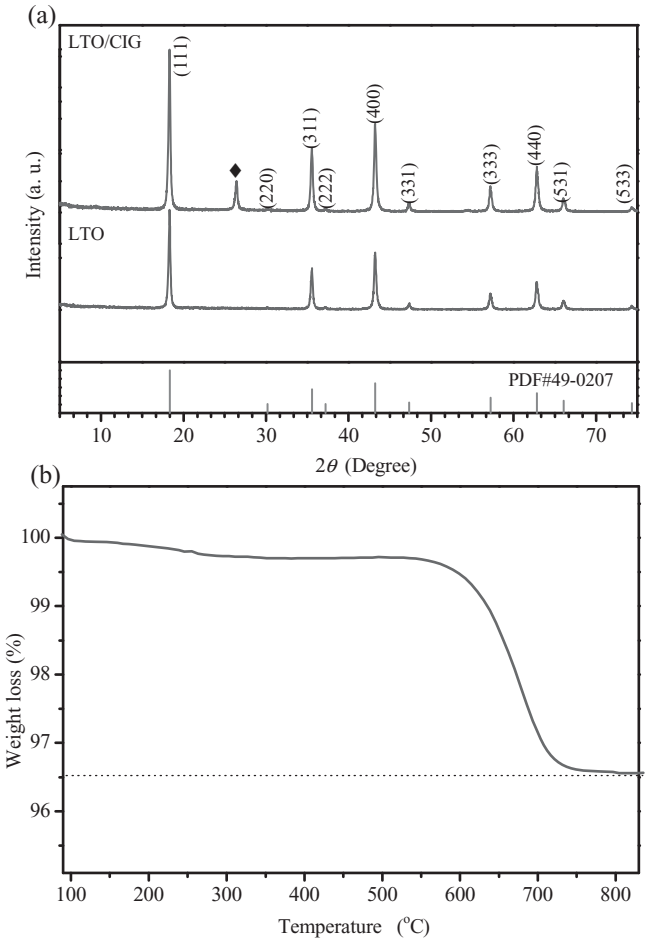

Figure 2. (a) XRD patterns of pure LTO and LTO/CIG samples. (b) TG analysis of LTO/CIG composite sample.

The morphology and structure of the pure LTO and LTO/CIG composite samples were further elucidated using TEM. **Figure 3**a and b show typical transmission electron microscopy (TEM) images of pure LTO and LTO/CIG composite. By comparing with the pure LTO, it can be seen clearly that the LTO nanoparticles are uniformly distributed between the cathodically induced graphene, by which graphene restacking and LTO nanoparticles aggregation can be prevented. The grain size of LTO particles in composite is about 20–50 nm (Figure 3b), which is noticeably smaller than that of pure LTO (Figure 3a, 50–100 nm). From the high resolution TEM images (Figure 3c and d), a lattice fringe of LTO about 0.21 nm is clearly observed, which is in good agreement with the spacing of the (400) planes of spinel $Li_4Ti_5O_{12}$. Additionally, it can be found that the LTO particles in composite (Figure 3d) are uniformly attached on the graphene layers.

Figure 3e and f show the N_2 adsorption/desorption isotherms and the pore size distribution of the pure LTO and LTO/CIG composite. As can be seen, the two isotherms with distinct hysteresis loops at high pressures can be identified as type-IV.[43] The specific surface area of LTO/CIG sample (13.6 m^2 g^{-1}) is only slightly higher than that of pure LTO sample (12.3 m^2 g^{-1}), this may due to the high loading amount of LTO in composite (3.5 wt.%). The pore size distribution (insets of Figure 3e and f) was obtained from the isotherm adsorption branches based on Barrett-Joyner-Halenda (BJH) model. There are two peaks at 2.4 nm and 10.6 nm for LTO/CIG, while only a narrow peak at 2.4 nm for pure LTO, which can be ascribed to the gaps between LTO nanoparticles and graphene sheets.

2.2. Electrochemical Properties

The electrochemical performance of the fabricated LTO/CIG composite was systematically evaluated using the coin-type cell configuration, and the results were compared with that of pure LTO. The cycling behavior of LTO/CIG at high rates of 0.5 C (1 C = 175 mA g^{-1}), 10 C and 25 C within the voltage range of 1–3 V were shown in **Figure 4**a, and the results for pure LTO electrode was also included for comparison (Figure 4b). As it can be seen, the initial reversible discharge specific capacities of LTO/CIG at 0.5, 10 and 25 C (charge and discharge at the same rate) are 174.7, 162.5 and 151.5 mAh g^{-1}, respectively. The retained capacities for 0.5, 10, and 25 C after 500 cycles are 168.1, 146.8 and 113.0 mAh g^{-1}, and the retention ratios are 96.2, 90.3 and 74.6%, respectively. It should be noted that the Coloumbic efficiency of this composite during cycling is over 99.5% (Figure 4c). Referring to pure LTO, the initial reversible discharge specific capacity at 0.5, 10 and 25 C are only 166.5, 125.5 and 73.6 mAh g^{-1}, and retention ratios after 500 cycles are only 91.6, 81.5 and 34.3%. These results confirmed that the lithium titanate tailored by cathodically induced graphene here own high specific capacity and excellent cycling stability at high rate charge/discharge.

Figure 4d compared the rate performance between the pure LTO and LTO/CIG. It is clear that the LTO/CIG sample exhibits improved rate performance that the pure LTO sample. At a high rate of 100 C (charge/discharge in 36 s, 17.5 A g^{-1}), a specific capacity of 126 mAh g^{-1} can be retained for LTO/CIG composite sample which is 72% of the theoretical capacity. In contrast, for pure LTO, the specific capacity decline quickly to 90 mAh g^{-1} at a rate of 25 C. A Ragone plot shown in **Figure 5** was used to evaluate the advantage of our high power anode materials. The plot shows higher specific-power and specific-energy density values for the LTO tailored by cathodically induced graphene/Li half cells in relation to that of LTO. At low power of 136 W kg^{-1}, the LTO/CIG composite and LTO can deliver a specific energy of 272 and 243 Wh kg^{-1}, respectively. LTO/CIG composite sample stores 246 Wh kg^{-1} of energy even at high power of 2600 W kg^{-1} (10 C) against only 175 Wh kg^{-1} for LTO sample at the same power. Remarkably, even during 36 s of charge/discharge (100 C), the LTO/CIG composite sample exhibits 166 Wh kg^{-1} of energy which is about 61% of the energy at 0.5C. **Figure 6**a shows the charge/discharge curves of LTO/CIG and pure LTO samples at various rates from 0.5 to 100C. Both the samples show long flat potential plateaus at different current rates, which ensure a constant voltage output, a key issue for LIBs. The rate capabilities of LTO/CIG and pure LTO samples are also shown in Figure 6b for comparison. The LTO/CIG sample can deliver a discharge specific capacity of 174, 171, 166 and 162 mAh g^{-1} using a charge and discharge rate of 0.5, 1, 5, and 10 C, respectively. Even charge/discharge

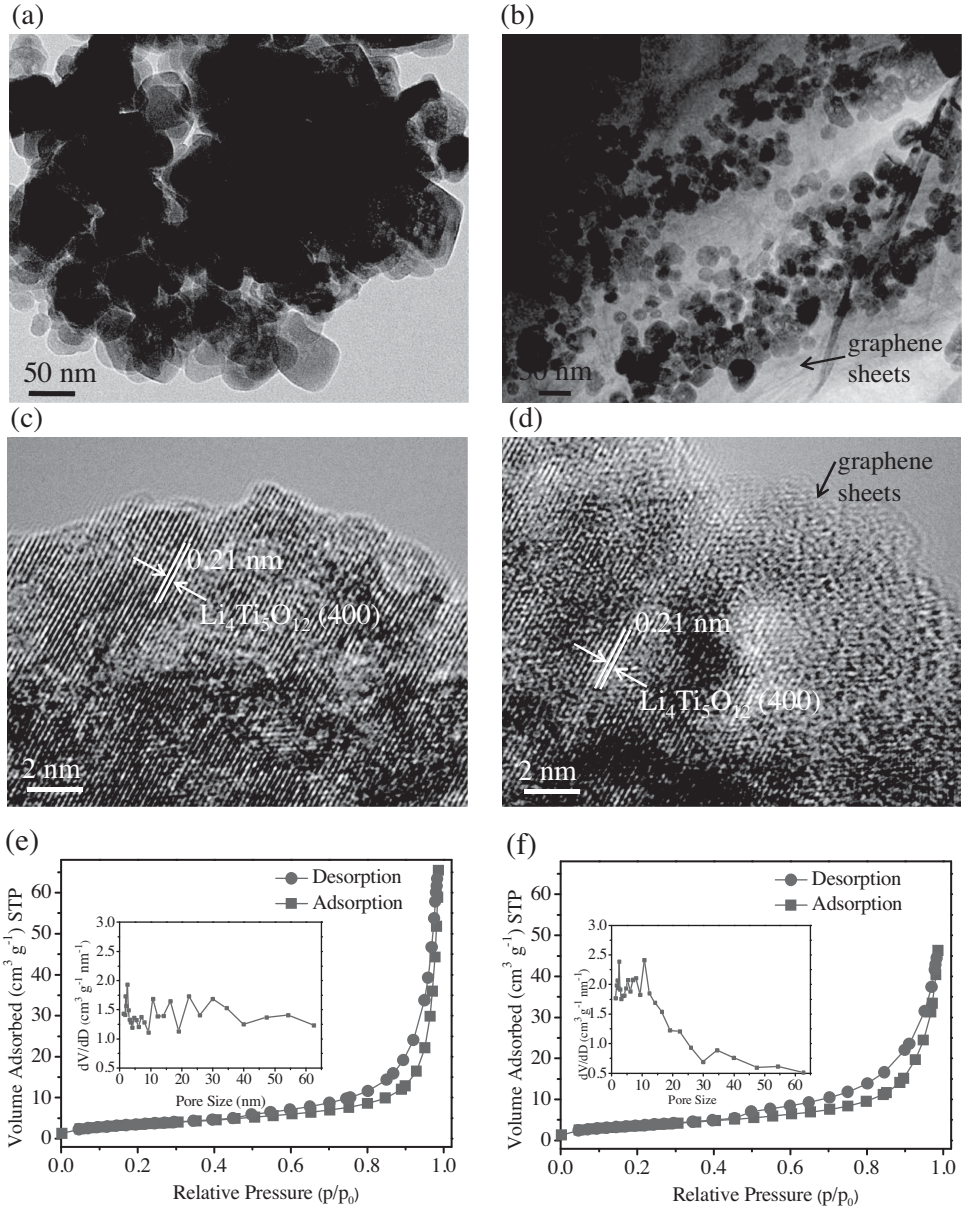

Figure 3. (a,b) Typical TEM and (c,d) HRTEM images of (a,c) pure LTO and (b,d) LTO/CIG composite samples. The nitrogen adsorption–desorption isotherm (inset: pore size distribution) of (e) pure LTO and (f) LTO/CIG composite samples.

at high rates of 25, 50, 80 and 100 C, the composite sample can still carry a discharge specific capacity of 154, 146, 136 and 126 mAh g^{-1}. For pure LTO sample, it can only deliver a discharge specific capacity of 159 mAh g^{-1} at 0.5 C, and the capacities drop rapidly to 148, 135, 119, and 90 mAh g^{-1} at 1, 5, 10 and 25 C, respectively. Taking the LTO materials reported so far for comparison (**Table 1**), the as-prepared LTO/CIG composite here exhibits excellent cycling stability and marvelous rate capability.

2.3. Understanding the Role of CIG

To evaluate LIB performances, the electrochemical polarization is one of the most important factors.[44] It is well known that with a voltage difference of >250 mV, over 30% of the energy is lost through heat.[45] Figure 6c shows the polarization of voltage difference (ΔE, the values of ΔE are define as the difference between the voltages of charge plateaus and discharge plateaus)[44,45] versus rate plots of the LTO/CIG and pure LTO samples. With inherent poor electrical conductivity of LTO, an increase of ΔE as a function of rate can be clearly observed in these samples. In comparison with other LTO materials (Table 1), the as-prepared LTO/CIG composite materials here show relatively low ΔE (105 mV) at charge/discharge rate of 10 C. It could be explained by the huge electrical conductivity of the LTO/CIG composite (1.2×10^{-4} S cm^{-1}), which is about 10^7 times higher than that of pure LTO sample (10^{-11} S cm^{-1}). Also, the EIS tests of LTO/CIG composite and the pure LTO

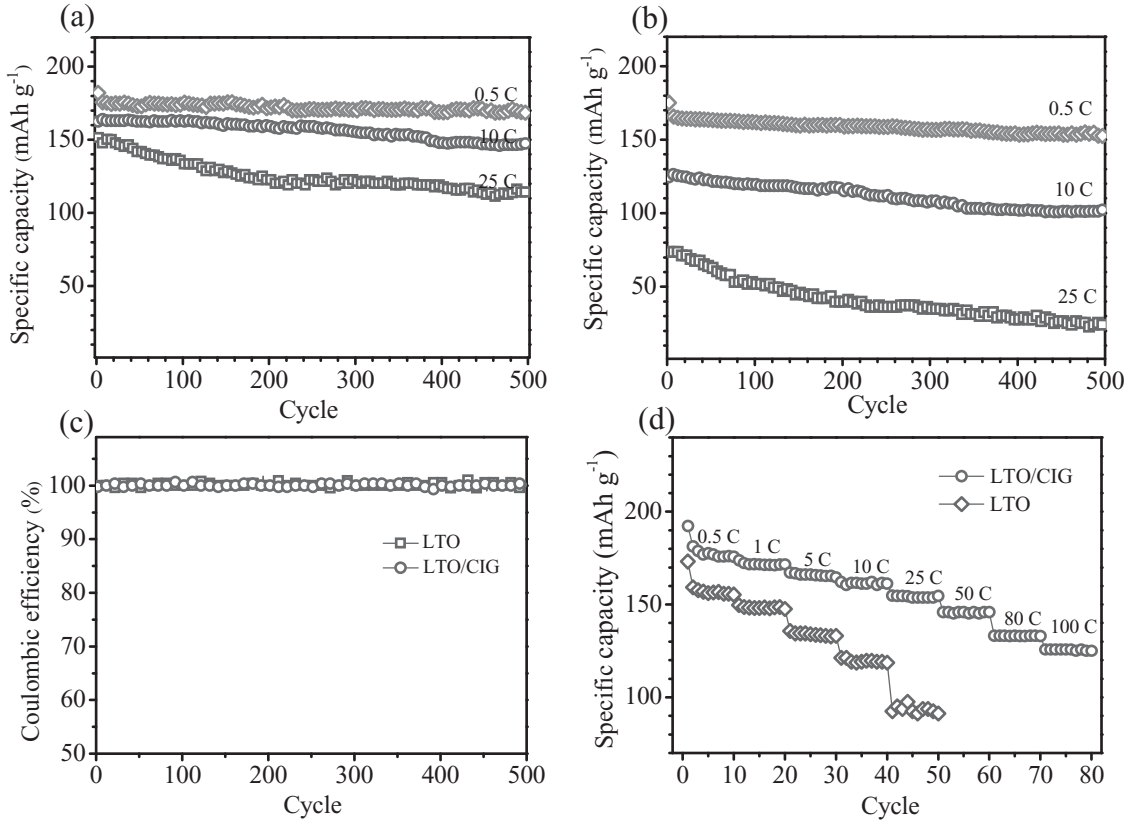

Figure 4. Cycling performance of (a) LTO/CIG composite and (b) pure LTO at 0.5, 10 and 25C. (c) Coulombic efficiency and (d) rate performance of LTO/CIG composite and pure LTO.

electrodes were shown in **Figure 7**. Generally, the intercep at the Z′ axis in the high frequency region is attributed to the ohmic resistance of electrode and electrolyte, and the semicircle in the medium-frequency range is attributed to the Li^+ charge-transfer impedance on the electrode–electrolyte interface.[22,41] According to the modified Randles equivalent circuit given in the inset of Figure 7, the charge-transfer impedance (R_{ct}) of LTO/CIG electrode is 19.9 Ω, which is about three times lower than that of pure LTO electrode (54.7 Ω). This indicates that the introducing of cathodically induced graphene in LTO/CIG composite here considerably improves the electrical conductivity of LTO/CIG composite and relieves the polarization of the electrode, which could contribute to the enhanced rate capability.

The electrochemical reaction of LTO with Li^+ is shown in the following equation:

$$Li_4Ti_5O_{12} + xLi^+ + xe^- \leftrightarrow Li_{4+x}Ti_5O_{12} (0 < x \leq 3) \quad (1)$$

The reaction occurs only when equivalent electrons and ions and are available simultaneously.[46] Thus, LTO materials with an excellent rate charge and discharge capability should have both high electronic conductivity and lithium ion diffusion coefficient. The electronic conductivity is an assessment of the ability to accept electrons, while lithium ion diffusion coefficient is a reflection of the speed of Li-ion diffusion. To clarify the effects of cathodically induced graphene incorporating agents on the lithium ion diffusion coefficient of the LTO/CIG composite electrode, cyclic voltammetry (CV) was also conducted on the LTO/CIG composite (**Figure 8**b) and the pure LTO (Figure 8a) electrodes at various scan rates. With increasing the scan rate, the intercalation and deintercalation peaks shift to low and high potentials, respectively. However, the LTO/CIG electrode (Figure 8b) shows smaller potential shifts between the intercalation and deintercalation peaks than that of LTO electrode (Figure 8a), showing improved electrode

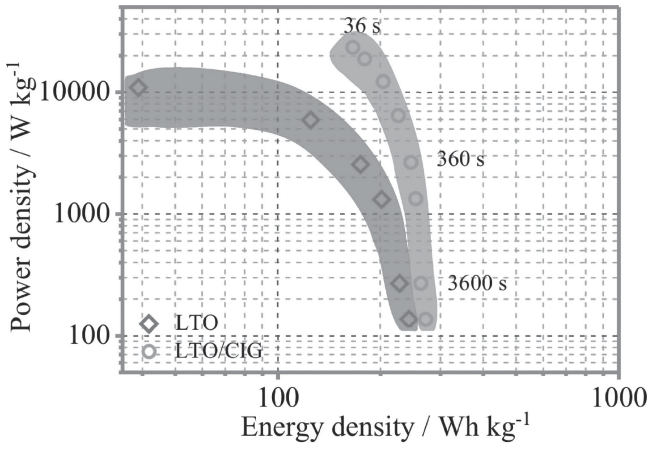

Figure 5. Ragone plot for LTO/CIG composite and pure LTO.

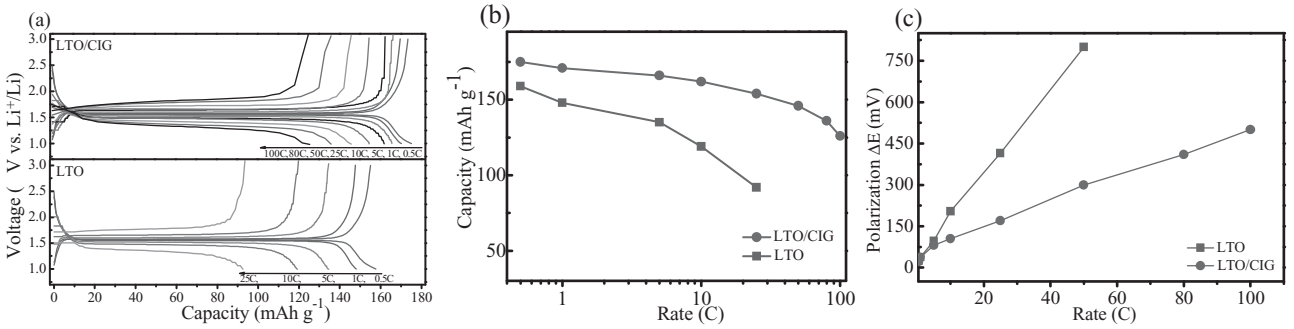

Figure 6. (a) Galvanostatic discharge/charge voltage profiles at different rates, (b) rate capability and (c) plots of ΔE versus C rates of LTO/CIG composite and pure LTO.

kinetics by incorporating cathodically induced graphene. As shown in insets of Figure 8, the peak current (i_p) exhibits a linear relationship with the square root of the scan rate ($\upsilon^{1/2}$), which is considered as a diffusion-controlled progress rather the surface control. It is notable that the Li^+ chemical diffusion coefficient in EC/DMC solutions (ca. 1.39×10^{-5} cm^2 s^{-1}) is much higher than the diffusion coefficient in solid-state LTO body (10^{-10}~10^{-13} cm^2 s^{-1}).[16–18,47] Thus, the rate-controlling step during charge/discharge is the diffusion of Li^+ in solid-state LTO electrode. From the relationship shown in insets of Figure 8, the apparent Li-ion chemical diffusion coefficient (D) in the electrode can be determined using the Randles–Ševčík equation (Equation (2)) [48,49]

$$i_p = 0.4463n^{3/2}F^{3/2}R^{-1/2}T^{1/2}SD^{1/2}C_{Li^+}\upsilon^{1/2} \quad (2)$$

where n, F, R, T, S and C_{Li+} is the charge transfer number, the Faraday constant, the gas constant, the absolute temperature, the surface area of the electrode and the concentration of Li^+, respectively. It was deduced that the LTO/CIG electrode could give apparent Li-ion chemical diffusion coefficient values of 1.61×10^{-12} cm^2 s^{-1}, which is approximately six times larger than 2.63×10^{-13} cm^2 s^{-1} of LTO electrode. The results above should be attributed to the smaller LTO particles and less aggregation between the particles as a result of the presence of defect-free cathodically induced graphene.

3. Conclusion

Nonoxidative cathodically induced graphene has been introduced to tailor the structure of $Li_4Ti_5O_{12}$ utilising controlled hydrolysis of tetrabutyl titanate in the presence of CIG and

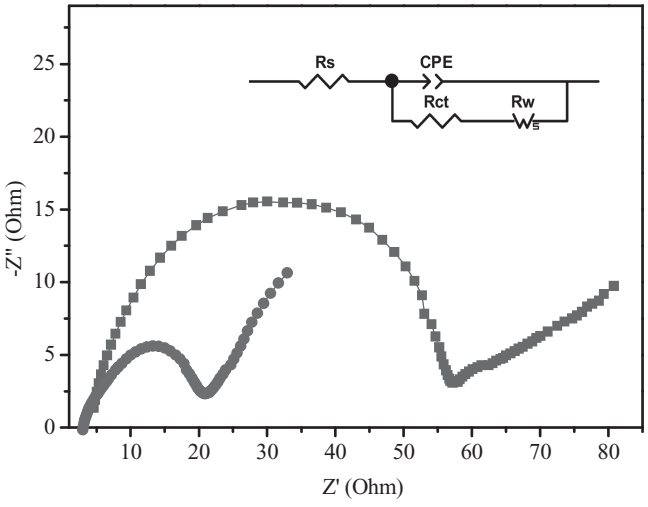

Figure 7. Electrochemical impedance spectroscopy of the LTO/CIG composite and pure LTO.

Table 1. High rate performance, cycling performance and polarization of voltage difference (ΔE) of the structured $Li_4Ti_5O_{12}$ (LTO) materials or LTO composite materials prepared through wet chemical synthesis.

Compound	10C capacity [mAh g^{-1}]	100 C capacity [mAh g^{-1}]	Capacity retention at 10 C	Polarization at 10 C [mV]
Hydrogenated LTO Nanowire[22]	157	121 (30 C)	95% over 100 cycles (5 C)	/
LTO/graphene nanosheets[30]	~135	82.7 (60 C)	97.5% over 100 cycles	~225
Cubic LTO/carbon composite[41]	151	134.9 (20 C)	80.3% over 200 cycles	~330
N-doped carbon coating LTO[44]	~152	~123	98.5% over 100 cycles	200
LTO/reduced graphite oxides[29]	~145	100	96% over 100 cycles	~120
TiO_2 nanocoated LTO[18]	~160	110 (60 C)	>98% over 100 cycles	~150
Carbon-encapsulated F-doped LTO[26]	123	91 (60 C)	>95.8% over 200 cycles (1 C)	/
Pure LTO (this work)	120	/	82.6% over 500 cycles	204
LTO/CIG (this work)	162	126	90.7% over 500 cycles	105

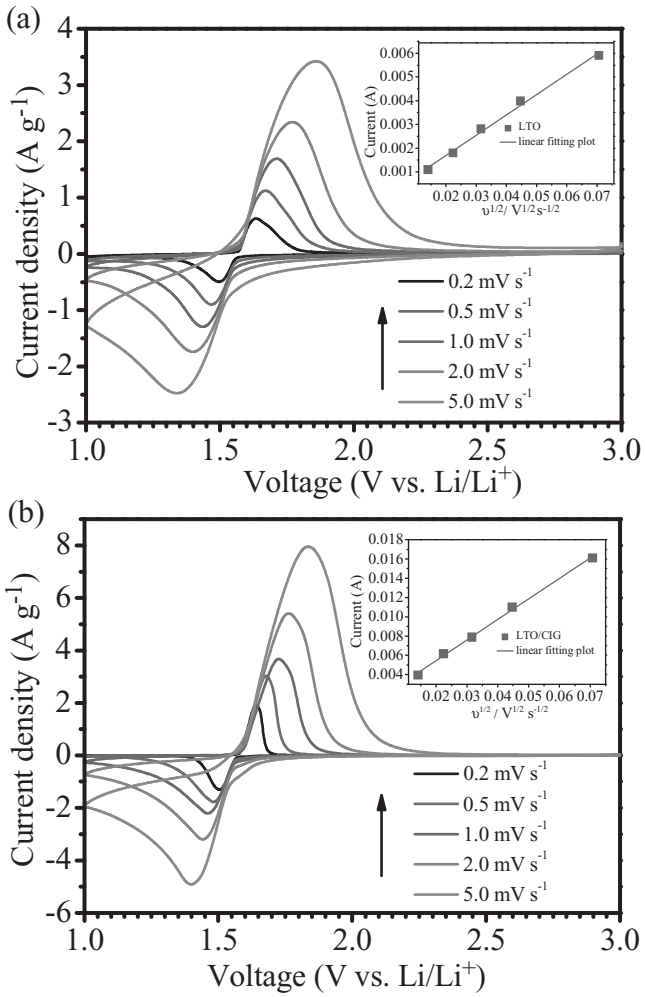

Figure 8. CV plots of the (a) pure LTO and (b) LTO/CIG composite at various scan rates ranging from 0.2 to 5.0 mV s^{-1}. Insets: the linear relationship of peak current (i_p) and the square root of the scan rate ($\upsilon^{1/2}$).

oxalic acid in a mixed solvent of ethanol and water followed by hydrothermal reaction and calcinations treatment. The designed LTO/CIG with uniform LTO particles demonstrates lower polarization of voltage difference, higher electrical conductivity (1.2×10^{-4} S cm^{-1}) and lithium ion diffusion coefficient (1.61×10^{-12} cm^2 s^{-1}) than that of pure LTO, when used as anodes materials in Li ion batteries. Thus, the electrochemical performances of LTO/CIG composite, including cycling stability and rate capability, have been largely enhanced in comparison with the most of LTO materials. This strategy paves a road for the exploitation of high energy density and high power density materials for lithium ion battery used in future electric vehicles and stationary off-peak energy storage systems.

4. Experimental Section

Synthesis of Pure LTO and LTO/CIG: Cathodically induced graphene (CIG) were prepared by electrochemically cathodic exfoliation in room temperature ionic liquids N-butyl, methylpyrrolidinium bis(trifluoromethylsulfonyl)imide (BMP-TF2N) described in our previous results.[38] In a typical synthesis, 5 g $Ti(OC_4H_9)_4$ (tetrabutyl titanate, TBT) and 0.5 g of acetic acid were dissolved in 50 mL ethanol. Then, the mixture was dropwise added into 50 mL of water/ethanol solution (1:1, in volume) containing 2 g of oxalic acid (OA), and 0.1 g of CIG under stirring at 50 °C. After being further stirred for 3 h, the resulting gray precipitate was collected by filtration and repeatedly washed with deionized water and ethanol, and then dried at 50 °C. Then 0.3 g composite power dispersed in 50 mL aqueous solutions of 1.0 M LiOH was transferred into Teflon-lined stainless steel autoclave and kept at 120 °C for 24 h. After cooling down naturally, the precipitate was harvested by filtration and washed thoroughly with ethanol and deionized water several times. The products were further dried at 50 °C for 12 h. Subsequently, the as-obtained agglomerate precursor composite was calcined at 800 °C under Ar for 1 h to obtain crystalline LTO/CIG. For comparison, pure LTO was synthesized without using CIG under the same condition.

Materials Characterization: High-resolution transmission electron microscopy (HRTEM) analysis was conducted a JEM-2100F instrument with an accelerating voltage of 200 kV. The Brunauer-Emmett-Teller (BET, BELSORP-MINI II) specific surface area was obtained from the N_2 adsorption/desorption isotherm recorded at 77K and the pore size distribution was evaluated by using the Barrett-Joyner-Halenda (BJH) model. X-ray diffraction (XRD) patterns were obtained with a Rigaku D/max 2550 VB+ 18kW X-ray diffractometer with Cu Kα radiation (0.1542 nm). Thermogravimetric analysis (TGA) data were collected on a thermal analysis instrument (NETZSCH STA449F3) with a heating rate of 10 °C min^{-1} from room temperature to 850 °C in air. The DC electrical conductivity of LTO/CIG composite was measured by a four-point probe conductivity measurement (SDY-40, Guangdong, China), in which disk sample was contacted with a four-point probe.

Electrochemical Measurements: Active materials dried at 50 °C for 24 h in a vacuum oven were mixed with a binder poly(vinylidenefluoride) (PVdF) and acetylene black at weight ratios of 80:10:10 in N-methyl-2-pyrrolidone (NMP) solvent to form a slurry. Then, the resultant slurries were uniformly pasted on Cu foil with a blade. The average mass of the active material in the prepared electrode sheets is 1.3 mg cm^{-1}. These prepared electrode sheets were dried at 100 °C in a vacuum oven for 12 h and pressed under a pressure of approximately 20 MPa. CR2016-type coin cells were assembled inside an mBraun glovebox (H_2O < 0.5 ppm, O_2 < 0.5 ppm) using the metallic lithium counter/reference electrode, a polypropylene separator (Celgard 2400), an electrolyte of 1 M $LiPF_6$ in ethylene carbonate and dimethyl carbonate (EC/DMC, 1:1 vol). Galvanostatic charge/discharge cycles were carried out with an Arbin battery cycler (BT2000) between 3.0 and 1.0 V vs Li^+/Li. The electrochemical impedance measurements were performed on Solartron Analytical at an AC voltage of 5 mV amplitude in the frequency range of 10^5 ~ 10^{-2} Hz. Cyclic voltammetry (CV) tests were also conducted on Solartron Analytical between 1.0 and 3.0 V at scan rates of 0.2, 0.5, 1.0, 2.0 and 5.0 mV s^{-1}.

Acknowledgements

Financial supports from the NNSF of China (No. 21003161, 21250110060), Funds for Distinguished Young Scientists of Hunan Province, China (No. 13JJ1004) and Fundamental Research Funds for the Central Universities of Central South University (No. 2012zzts059) are greatly appreciated.

Received: December 23, 2013
Revised: February 6, 2014
Published online: April 1, 2014

[1] J. M. Tarascon, M. Armand, *Nature* **2001**, *414*, 359.
[2] M. Armand, J. M. Tarascon, *Nature* **2008**, *451*, 652.
[3] J. B. Goodenough, K.-S. Park, *J. Am. Chem. Soc.* **2013**, *135*, 1167.
[4] M. V. Reddy, G. V. Subba Rao, B. V. R. Chowdari, *Chem. Rev.* **2013**, *113*, 5364.

[5] V. Etacheri, R. Marom, R. Elazari, G. Salitra, D. Aurbach, *Energy Environ. Sci.* **2011**, *4*, 3243.
[6] P. Yu, B. N. Popov, J. A. Ritter, R. E. White, *J. Electrochem. Soc.* **1999**, *146*, 8.
[7] Y.-K. Sun, S.-T. Myung, B.-C. Park, J. Prakash, I. Belharouak, K. Amine, *Nat. Mater.* **2009**, *8*, 320.
[8] S. Yang, X. Feng, K. Müllen, *Adv. Mater.* **2011**, *23*, 3575.
[9] H.-G. Jung, M. W. Jang, J. Hassoun, Y.-K. Sun, B. Scrosati, *Nat Commun* **2011**, *2*, 516.
[10] T.-F. Yi, L.-J. Jiang, J. Shu, C.-B. Yue, R.-S. Zhu, H.-B. Qiao, *J. Phys. Chem. Solids* **2010**, *71*, 1236.
[11] E. Ferg, R. J. Gummow, A. de Kock, M. M. Thackeray, *J. Electrochem. Soc.* **1994**, *141*, L147.
[12] W. J. H. Borghols, M. Wagemaker, U. Lafont, E. M. Kelder, F. M. Mulder, *J. Am. Chem. Soc.* **2009**, *131*, 17786.
[13] G.-N. Zhu, Y.-G. Wang, Y.-Y. Xia, *Energy Environ. Sci.* **2012**, *5*, 6652.
[14] Z. Chen, I. Belharouak, Y. K. Sun, K. Amine, *Adv. Funct. Mater.* **2013**, *23*, 959.
[15] V. Manev, T. Spitler, M. Stewart, J. Shelburne, (Altairnano). US 20100178556-A1, **2010**.
[16] M. Wagemaker, E. R. H. van Eck, A. P. M. Kentgens, F. M. Mulder, *J. Phys. Chem. B* **2008**, *113*, 224.
[17] S. Takai, M. Kamata, S. Fujine, K. Yoneda, K. Kanda, T. Esaka, *Solid State Ionics* **1999**, *123*, 165.
[18] Y.-Q. Wang, L. Gu, Y.-G. Guo, H. Li, X.-Q. He, S. Tsukimoto, Y. Ikuhara, L.-J. Wan, *J. Am. Chem. Soc.* **2012**, *134*, 7874.
[19] Y.-B. He, B. Li, M. Liu, C. Zhang, W. Lv, C. Yang, J. Li, H. Du, B. Zhang, Q.-H. Yang, J.-K. Kim, F. Kang, *Sci. Rep.* **2012**, DOI: 10.1038/srep00913.
[20] J. M. Feckl, K. Fominykh, M. Döblinger, D. Fattakhova-Rohlfing, T. Bein, *Angew. Chem. Int. Ed.* **2012**, *51*, 7459.
[21] Y. Sha, B. Zhao, R. Ran, R. Cai, Z. Shao, *J. Mater. Chem. A* **2013**, *1*, 13233.
[22] L. Shen, E. Uchaker, X. Zhang, G. Cao, *Adv. Mater.* **2012**, *24*, 6502.
[23] Y. F. Tang, L. Yang, Z. Qiu, J. S. Huang, *Electrochem. Commun.* **2008**, *10*, 1513.
[24] L. Yu, H. B. Wu, X. W. Lou, *Adv. Mater.* **2013**, *25*, 2296.
[25] M. R. Jo, K. M. Nam, Y. Lee, K. Song, J. T. Park, Y.-M. Kang, *Chem. Commun.* **2011**, *47*, 11474.
[26] Y. Ma, B. Ding, G. Ji, J. Y. Lee, *ACS Nano* **2013**, *7*, 10870.
[27] C. Lee, X. Wei, J. W. Kysar, J. Hone, *Science* **2008**, *321*, 385.
[28] D. A. C. Brownson, D. K. Kampouris, C. E. Banks, *Chem. Soc. Rev.* **2012**, *41*, 6944.
[29] H.-K. Kim, S.-M. Bak, K.-B. Kim, *Electrochem. Commun.* **2010**, *12*, 1768.
[30] L. Shen, C. Yuan, H. Luo, X. Zhang, S. Yang, X. Lu, *Nanoscale* **2011**, *3*, 572.
[31] Y. Tang, F. Huang, W. Zhao, Z. Liu, D. Wan, *J. Mater. Chem.* **2012**, *22*, 11257.
[32] M. J. Allen, V. C. Tung, R. B. Kaner, *Chem. Rev.* **2009**, *110*, 132.
[33] C. Gómez-Navarro, R. T. Weitz, A. M. Bittner, M. Scolari, A. Mews, M. Burghard, K. Kern, *Nano Lett.* **2007**, *7*, 3499.
[34] S. Stankovich, D. A. Dikin, G. H. B. Dommett, K. M. Kohlhaas, E. J. Zimney, E. A. Stach, R. D. Piner, S. T. Nguyen, R. S. Ruoff, *Nature* **2006**, *442*, 282.
[35] W. Song, X. Ji, W. Deng, Q. Chen, C. Shen, C. E. Banks, *Phys. Chem. Chem. Phys.* **2013**, *15*, 4799.
[36] W. Deng, X. Ji, M. Gomez-Mingot, F. Lu, Q. Chen, C. E. Banks, *Chem. Commun.* **2012**, *48*, 2770.
[37] J. Wang, K. K. Manga, Q. Bao, K. P. Loh, *J. Am. Chem. Soc.* **2011**, *133*, 8888.
[38] Y. Yang, F. Lu, Z. Zhou, W. Song, Q. Chen, X. Ji, *Electrochim. Acta* **2013**, *113*, 9.
[39] W. Wen, X. Huang, S. Yang, K. Lu, P. Sheng, *Nat. Mater.* **2003**, *2*, 727.
[40] T.-T. Fang, H.-B. Lin, J.-B. Hwang, *J. Am. Ceram. Soc* **1990**, *73*, 3363.
[41] B. Li, C. Han, Y.-B. He, C. Yang, H. Du, Q.-H. Yang, F. Kang, *Energy Environ. Sci.* **2012**, *5*, 9595.
[42] S. J. R. Prabakar, Y.-H. Hwang, E.-G. Bae, S. Shim, D. Kim, M. S. Lah, K.-S. Sohn, M. Pyo, *Adv. Mater.* **2013**, *25*, 3307.
[43] Y. Wang, H. Rong, B. Li, L. Xing, X. Li, W. Li, *J. Power Sources* **2014**, *246*, 213.
[44] N. Li, G. Zhou, F. Li, L. Wen, H.-M. Cheng, *Adv. Funct. Mater.* **2013**, *23*, 5429.
[45] X. Hao, B. M. Bartlett, *Adv. Energy Mater.* **2013**, *3*, 753.
[46] L. Sun, J. Wang, K. Jiang, S. Fan, *J. Power Sources* **2014**, *248*, 265.
[47] S.-I. Lee, U.-H. Jung, Y.-S. Kim, M.-H. Kim, D.-J. Ahn, H.-S. Chun, *Korean J. Chem. Eng.* **2002**, *19*, 638.
[48] W. Song, X. Ji, C. Pan, Y. Zhu, Q. Chen, C. E. Banks, *Phys. Chem. Chem. Phys.* **2013**, *15*, 14357.
[49] C.-Y. Wu, Y.-X. Wang, J. Xie, G.-S. Cao, T.-J. Zhu, X.-B. Zhao, *J. Solid State Electrochem.* **2012**, *16*, 3915.